ACS OMEGA

http://pubs.acs.org/journal/acsodf

Article

Ocimum sanctum Leaf Extract-Assisted Green Synthesis of Pd-Doped CuO Nanoparticles for Highly Sensitive and Selective NO_2 Gas Sensors

Anit K. Ambedkar, Durvesh Gautam, Sagar Vikal, Manohar Singh, Ashwani Kumar,* Amit Sanger, Kavita Sharma, Beer Pal Singh, and Yogendra K. Gautam*

Cite This: *ACS Omega* 2023, 8, 29663−29673

Read Online

ACCESS | Metrics & More | Article Recommendations

ABSTRACT: In view of facile, cost-effective, and environmentally friendly synthetic methods, palladium-doped copper oxide (Pd-CuO) nanoparticles have been synthesized from *Ocimum sanctum* (commonly known as "Tulsi") phytoextract for gas-sensing applications. The structural, morphological, and compositional properties of Pd-doped CuO nanoparticles were studied using various techniques such as XRD, FESEM, XPS, and EDX. The characterization results confirmed the doping of Pd on CuO nanoparticles, and Pd-CuO nanostructures appear as nanoflakes in FESEM analysis. The gas-sensing response of Pd (1.12 wt %)-CuO nanoflake-based sensor was measured at 5−100 ppm concentration of different gases, NO_2, H_2S, NH_3, and H_2, at 125 °C. Gas-sensing tests reveal that the sensitivity of the sensor were 81.7 and 38.9% for 100 and 5 ppm concentrations of NO_2, respectively, which was significantly greater than that of pure CuO. The response and recovery times of the sensor were 72 and 98 s for 100 ppm of NO_2 gas, while they were 90 and 50 s for 5 ppm NO_2. The calculated limit of detection (LOD) value of the sensor is 0.8235. This appealing LOD is suitable for real-time gas detection. The gas sensor was found to exhibit excellent selectivity toward NO_2 gas and repeatability and stability in humid (80%) conditions. The Pd doping in CuO nanostructures plays a significant role in escalating the sensitivity and selectivity of CuO-based NO_2 gas sensor suitable to work at low operating temperatures.

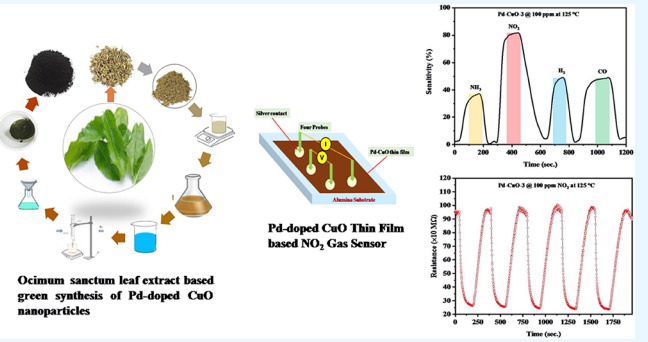

1. INTRODUCTION

Nitrogen dioxide (NO_2) is a noxious gas usually produced from the combustion of fossil fuels (coal, gas, and oil), refining of petroleum and metals, food manufacturing, making of nitric acid, welding, use of explosives, and other industrial activities.[1,2] Increased NO_2 levels can harm the human respiratory system and increase a person's vulnerability.[3,4] NO_2 is also related to some diseases such as olfactory paralysis, chronic lung disease, acute respiratory illness (asthma), and so on.[5−7] NO_2 gas not only has a negative impact on human health, but it also causes acid rain and photochemical smog.[1,8] Therefore, it is essential to detect NO_2 effectively for both environmental sustainability and human health. NO_2 gas can be detected via semiconductor metal oxide (SMO)-based sensing devices.[9] In addition to this, recently, detection of various other toxic gases such as carbon monoxide, toluene, xylene, and benzene has been studied via SMO-based high-performance sensing devices.[10−15] SMO-based NO_2 gas sensors are found to be the best among others because of its lower limit of detection, low cost, and vigorous detection. However, designing a high-performance NO_2 gas sensor in terms of selectivity, stability, and feasibility in various environmental conditions is still an open challenge for researchers. Nowadays, research has been aimed to enhance the selectivity, sensitivity, repeatability and long-term stability and reduce the response/recovery times of NO_2 gas sensors at lower temperatures.[16,17]

Recently, several attempts have been made to make efficient gas sensors for the detection of NO_2.[16] These studies demonstrate a mixed combination of SMOs, homojunctions, and heterojunctions of p−n, n−p, n−n, and p−p types of materials for NO_2 gas sensors, such as ZnO nanosheets,[16] CuO nanoparticles,[17] Ag-SnO_2-C_3N_4 ternary nanocomposites,[18] and so forth. Most of these SMO sensors for NO_2 detection have

Received: May 29, 2023
Accepted: July 19, 2023
Published: August 2, 2023

CuO as the core material, probably because of its good thermal stability and good oxygen adsorption.

Several researchers have worked toward improving the NO_2 gas sensor selectivity and sensitivity. Hou and Hsueh[19] reported a CuO nanosheet-/MEMS-based NO_2 sensor; the sensor shows good response at 50 ppb of NO_2 at various temperatures. Hung et al.[20] reported that n-WO_3/p-MWCNT nanocomposite-based NO_2 gas sensor demonstrated a response of 18% and response/recovery times of 87 s/300 s toward 5 ppm NO_2 at 150 °C. Jaiswal et al.[21] reported a pristine ZnO@PSi-based NO_2 sensor with a response value of 5.72% and response/recovery times of 41 s/124 s at 150 °C. Munusami et al.[22] reported that $ZnGa_2O_4$/graphene with the nanoplate hybrid structure showed good response to NO_2 gas; moreover, the selectivity, stability, sensitivity, and response/recovery times were better for LPG.

To enhance the gas-sensing characteristics such as selectivity, sensitivity, operating temperature, and response and recovery times, metal oxides were filled with nanoparticles of noble or catalytic metals on the surface. For example, Gawali et al.[23] prepared a 0.5% Ce-doped NiO thin-film NO_2 gas sensor that showed a maximum response of 71.9% for 1 ppm NO_2 at 150 °C. Zhang et al.[4] prepared a NO_2 gas sensor based on a 2% Al-doped narcissus-like ZnO nanostructure. The sensor presented excellent sensing performance, i.e., good sensing response (103.2% toward 1 ppm NO_2), shorter response/recovery times (53 s/21 s), and a lower detection limit (0.1 ppm). Khudadad et al.[24] reported that a NO_2 sensor based on WO_3 nanostructures showed a response of 392% toward 150 ppm at room temperature.

However, the sensing parameters, sensitivity, stability, response, recovery times, and so forth, of these sensors still need to be further enhanced to meet the criteria for practical applications at low working temperatures.[25]

Copper oxide (CuO) is a p-type SMO with a monoclinic crystal structure and a relatively small band gap of 1.7 eV.[26,27] CuO is naturally nontoxic and easily available with a low processing cost. Moreover, it has high thermal stability along with excellent optical, chemical, and electrical properties. In addition, CuO has potential applications in the field of solar cells,[28] batteries,[29] biosensors,[30] photocatalysts,[31] and gas sensors.[32] Only a few reports are available for CuO- or Pd-doped CuO nanostructures for toxic gas detection, particularly NO_2 gas. Oosthuizen et al.[33] reported a p-type CuO nanoplatelet-based NO_2 gas sensor with a remarkable response of 14.5% to 20 ppm NO_2 at room temperature. The selectivity and sensitivity of the CuO nanoplatelet-based NO_2 sensor were found to be reaction temperature- and time-dependent. Again, Oosthuizen et al.[34] prepared CuO nanoplatelets for NO_2 detection, which showed response values of ∼2498% to 40 ppm NO_2 gas, at room temperature in dry air conditions. Mali et al.[35] successfully synthesized CuO(50%)−ZnO(50%) nanocomposites (NCs) by a simple one-step chemical method. The sensor exhibited remarkable gas-sensing performance with superior selectivity toward NO_2 gas at 200 °C. Gomaa et al.[36] reported NiO thin-film gas sensors that showed a response of 57.3% toward 20 ppm NO_2 at 200 °C with good selectivity and stability. The facile hydrothermal-fabricated CuO/ZnO sensor showed a maximum sensitivity of 337% for 5 ppm of NO_2 gas, with response/recovery times of 18/32 s, and the detection limit is observed to be 155 ppb at RT (30 °C). The sensor exhibited a highly selective response to NO_2 gas compared to the other interfering gases (SO_2, N_2O, NH_3, and CO).[37] Mulberry-like Cu_2O/CuO composite-based sensors were synthesized by a one-pot hydrothermal process. The optimized Cu_2O/CuO composite exhibited outstanding selectivity, humidity tolerance, and stability toward NO_2.[38]

Utilizing plants and microbes in the synthesis of nanoparticles is a novel, cost-effective, and environment-friendly approach which can be ramped up for large-scale synthesis too.[25,39] Such synthesis methods are hassle-free as there is no need to use high pressure, energy, temperature, and toxic chemicals.[40,41] In addition, the green approach to synthesize SMO nanostructures allows to obtain nanoparticles with desirable size and better morphology. The merit of green-synthesized CuO-based system over the chemically synthesized system is that it not only decreases the risk to human health and environmental pollution but can also help to produce sensors with the appropriate microstructure that provides a remarkable response to the target gas.[42]

Various researchers have reported about the green synthesis of CuO nanoparticles from various plant extract such as *Aloe vera*,[43,44] *Terminalia phanerophlebia*,[45] *Gloriosa superba*,[46] *Psidium guajava*,[47] *Solanum nigrum*,[48] *Abutilon indicum*,[49] *Lantana camara*,[50] and *Malva sylvestris*.[51] This phytomediated method using different plant extracts is considered an innovative, low-cost, and modest approach for synthesizing CuO nanoparticles.

The doping of impurity ions is mainly to engineer the electrical and optical properties of CuO. Doping with Pd^{2+} cations in CuO is more efficient due to their nearly identical ionic radii, i.e., Cu^{2+} (0.73) and Pd^{2+} (0.86).[52] Hence, Pd^{2+} can be easily integrated into the CuO lattice without causing the crystal structure distortion.

In the present research, *Ocimum sanctum* (Tulsi) plant leaf extract was used as a reducing or capping agent for the green synthesis of CuO nanoparticles. This plant is abundantly found in tropical countries like India and possesses quite excellent medicinal properties. Researchers demonstrated that the size and surface morphology of the nanoparticles are strongly influenced by the plant material in the green synthesis.[53,54]

Very few reports are available on the green-synthesized nanostructure-based gas sensors. Goutham et al. compared the sensing performance of the ZnO-based sensor prepared by two different methods, i.e., green synthesis and chemical synthesis.[55] The chemically prepared ZnO-based sensor presented similar sensing properties as attained by the biosynthesized ZnO-based sensor. The fascinating electronic properties inspire biobased approaches which in turn cut down the environmental pollution.

Gattu et al.[56] reported the gas-sensing performance of biosynthesized pure SnO_2 and Ni-doped SnO_2 using Bengal gram beans (*Cicer arietinum*) extract for the detection of NO_2 gas at 200 °C. The Ni-doped SnO_2 sensor shows good response to NO_2. This may be due to the reduced particle size and increased specific surface area after the addition of Ni for the improved absorption of NO_2 gas. Moreover, their results showed that Ni-doped SnO_2 has excellent selectivity for detecting NO_2 in comparison to other H_2S, LPG, and NH_3 gases.

Gattu et al.[57] further investigated the sensing performance of an Au-doped SnO_2 thin film to NO_2 gas at an operating temperature of 200 °C. The obtained results demonstrate a gas response of about 30% to 100 ppm of NO_2. Thus, the biosynthesized Au-doped SnO_2 nanoparticle thin film-based

https://doi.org/10.1021/acsomega.3c03765
ACS Omega 2023, 8, 29663−29673

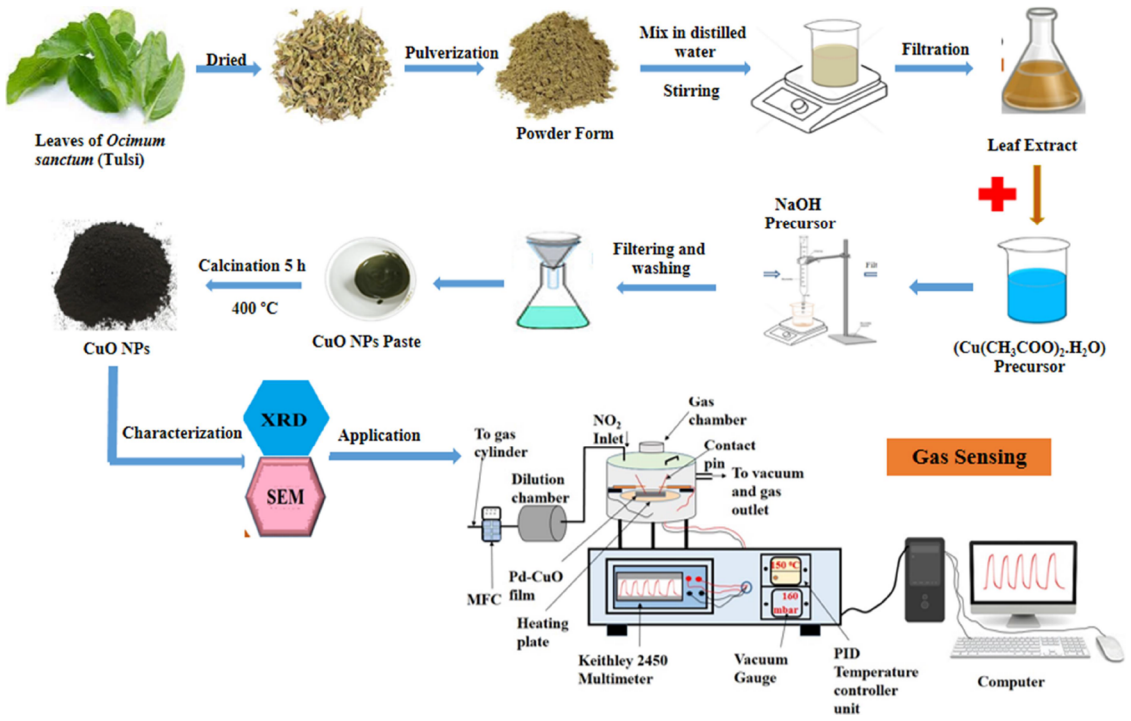

Figure 1. Schematic diagram showing the synthesis process of pure and Pd-CuO nanoparticles along with the gas-sensing setup.

sensor can be a promising solution for NO_2 gas sensing application.

Nagar et al.[58] reported green ZnO nanoparticles synthesized by using Parthenium hysterophorus leaf extract, which showed a response value of 2.5 and response/recovery times of 5 s/8 s toward 5 ppm NH_3 at room temperature. Recently, Poonguzhali et al.[59] synthesized natural lemon extract-assisted spinel Co_3O_4 nanoparticles. The sensor exhibits good sensing performance to 1000 ppm of LPG at 250 °C.

The present article encompasses a detailed study on NO_2 gas sensing performance of green-synthesized Pd-doped CuO nanostructures. The Pd dopants enhanced the sensing performance for NO_2. The possible sensing mechanism responsible for the vast improvement in sensing parameters is also investigated in the study. This highly sensitive and selective sensor is capable for NO_2 detection even at low operating temperatures. The article can possibly be an attempt to abate the air pollution by detecting the enhanced levels of NO_2 in the atmosphere via nontoxic, environment-friendly, economic, and, moreover, the sustainable biological source-assisted CuO nanoparticle-based NO_2 sensors.

2. EXPERIMENTAL SECTION

2.1. Synthesis of Pure and Pd-CuO Nanoparticles. *2.1.1. Preparation of Ocimum sanctum (Tulsi) Leaf Extract.* At first, *Ocimum sanctum* leaves were thoroughly cleaned to remove dust particles and then dried in sunlight to get rid of any remaining moisture. For preparing *Ocimum sanctum* leaf extract, 6 g of leaf powder was combined with 100 mL of distilled water in a 250 mL glass beaker; then, the mixture was boiled for 60 min at 85 °C with constant stirring (650 rpm). The mixture was filtered and then allowed to cool up to room temperature.

2.1.2. Preparation of CuO and Pd-Doped CuO Nanoparticles. CuO nanoparticles were prepared by the sol−gel method by using copper acetate ($Cu(CH_3COO)_2{\cdot}H_2O$), sodium hydroxide (NaOH), and *Ocimum sanctum* leaf extract. 0.3 M (5.989 g) copper acetate is combined with 100 mL of distilled water in a 200 mL beaker. After heating the mixed solution at 27 °C with constant stirring (600 rpm), 10 mL of *Ocimum sanctum* leaf extract is added to the mixture of copper acetate solution and stirred for 2 h. 0.2 M sodium hydroxide (NaOH) solution was prepared in a separate beaker and added dropwise to the above mixture solution with the help of a burette. A black precipitate started to form slowly at the bottom of the beaker. The obtained black precipitate was washed five times with distilled water and filtered with the help of a filter paper. Thereafter, the obtained product was dried at 100 °C for 3 h and finally calcined at 400 °C for 5 h. To prepare Pd-CuO nanoparticles, a required amount of palladium chloride ($PdCl_2$) was mixed with the previously prepared copper acetate solution. The CuO nanoparticles contained Pd concentrations of 0, 0.5, 0.8, and 1.12 wt %, and samples were named as CuO, Pd-CuO-1, Pd-CuO-2, and Pd-CuO-3, respectively. The whole process to prepare pure CuO nanoparticles is shown in Figure 1.

2.2. Characterization. The phase and crystal structures of the prepared pure and Pd-CuO nanoparticles were investigated by XRD (Bruker AXS, D8 Advance) with CuKα radiation (λ = 1.5406 Å) in the 2θ range of 20−80°. The morphological analysis of the nanoparticles was investigated by FESEM (FEI, Quanta 200F) at an accelerating voltage of 15 kV. The composition of the CuO nanostructures was confirmed using EDX. XPS was performed to study the electronic spectra and doping of Pd in the CuO lattice.

2.3. Gas Sensor Fabrication. The following steps were taken to fabricate a gas sensor by using pure CuO and Pd-CuO nanoflakes. First, the sample powders were carefully mixed with a small amount of distilled water to create a paste, which was then applied to an alumina substrate (8 mm × 8 mm × 1 mm) to make a thin film/sensing layer. The thin films were dried at 350 °C for 5 h to improve the mechanical strength.

https://doi.org/10.1021/acsomega.3c03765
ACS Omega 2023, 8, 29663−29673

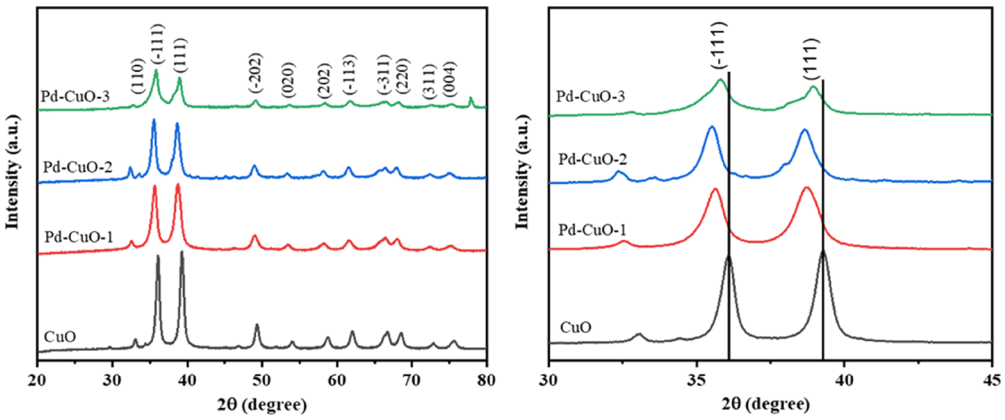

Figure 2. XRD patterns of the pure and Pd-CuO nanoparticles with different Pd concentrations.

After this, with the help of silver paste, four contacts were made on the surface of this sensing layer.[60]

2.4. Gas-Sensing Measurement. The gas-sensing properties of the developed sensor have been studied using a gas-sensing setup, as shown in Figure 1. The setup consists of a gas-sensing test system (Excel Instruments Co., Ltd., Maharashtra, India) with a 3 L stainless steel test chamber attached with a source meter (Keithley, 2450) and a PID controller (EXL-TC-2022-52) to heat the samples (range, RT−450 °C). The entire sample is heated at a constant rate of 0.1 °C/s. We have nitrogen balanced at 500 ppm; for the preparation of the desired gas concentration, the sample gas is mixed with dry air. For the gas-sensing performance of the sensor, first, atmospheric pressure was used to test the gas sensor's resistance. Then, a specific amount of gas was introduced into the chamber with the help of a magnetic valve. After measuring the resistance of the sensor in the presence of the gas, the gas was exhausted by an automatic magnetic valve.

3. RESULTS AND DISCUSSION

3.1. Morphological, Structural, and Chemical Analyses of Sensing Materials. Figure 2 shows the XRD patterns of pure and Pd-CuO nanoparticles. A well-defined diffraction peak can be seen in the CuO patterns at 2θ of 32.95, 36.11, 39.28, 49.33, 54.02, 58.79, 62.05, 66.69, 68.59, 72.91, and 75.68, corresponding to the (110), (−111), (111), (−202), (020), (202), (−113), (−311), (220), (311), and (004) planes of monoclinic CuO (JCPDS No. 72-0629). After Pd doping (0.5−1.12 wt %) in pure CuO, the peaks of planes (−111) and (111) are slightly shifted toward a lower angle, which means that the lattice constant changes, as shown in Figure 2. For the event that the ionic radius of Pd^{2+} (0.86 Å) is slightly larger than that of Cu^{2+} (0.73 Å), the replacement of Cu^{2+} by Pd^{2+} ions induces lattice expansion and thus shifts the peak to a lower angle. This clearly shows that the Pd^{2+} ions are doped into the CuO matrix successfully.

Figure 3 depicts the FESEM morphologies of pure and Pd-CuO nanostructures doped with various concentrations of Pd. As exhibited in Figure 3a, the pure CuO nanostructures have granular structures showing poor uniformity. Upon doping with 0.5 wt % Pd, the nanoparticle size increased slightly and the nanoparticle surface became smoother, as shown in Figure 3b. Such an increase, particularly at 0.5 wt %, is most likely due to morphological changes with larger diameters.[61] However, as the concentration of doping increased (0.8−1.12 wt %), the

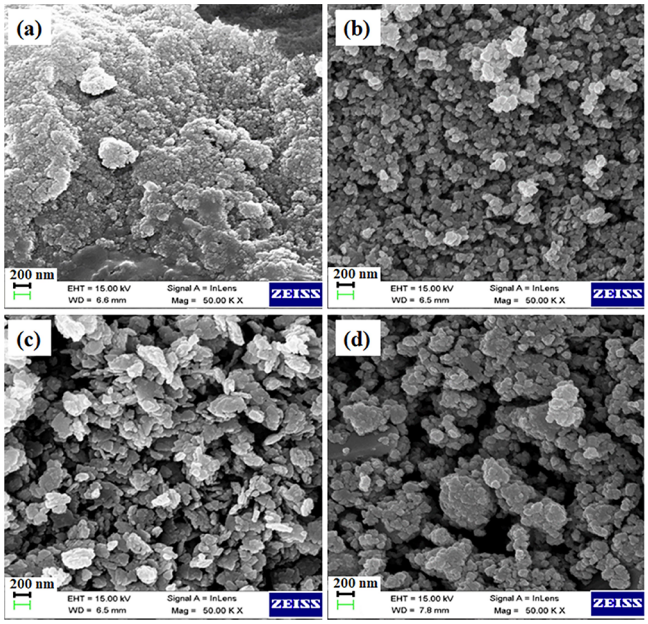

Figure 3. FESEM images: (a) pure CuO, (b) 0.5 wt % Pd-CuO, (c) 0.8 wt % Pd-CuO, and (d) 1.12 wt % Pd-CuO.

nanostructure changes from nanoparticles to nanoflakes along with the appearance of nanobars, as can be seen in Figure 3c,d.Thus, doping (Pd) plays an important role during the synthesis of CuO, and the resulting growth mechanism might be related to the preparation of metal oxides.[62]

The composition of CuO nanoparticles was further confirmed using EDX analysis. Figure 4 shows the EDX spectra of pure and Pd-CuO nanoparticles. It exhibits the presence of Cu, O, and Pd. Also, other peaks can be observed in the EDX spectra, which might be because of the plant leaf extract and conductive coating. Thus, EDX analysis confirms the findings of the XRD analysis.

XPS is a sensitive surface technique for examining the chemical compositions of surfaces.[63] A complete XPS survey spectrum of the 1.12 wt % Pd-CuO nanoparticles (Pd-CuO-3 sample) is shown in Figure 5a. The XPS peaks were found related to Cu, C, Pd, and O. The C 1s peak is related to the dust in air, while the other peaks are attributed to the sample. In the Cu 2p core-level XPS spectrum (Figure 5b), the peaks at 933.53 and 953.44 eV may be attributed to Cu $2p_{3/2}$ and Cu $2p_{1/2}$, respectively. The strong satellite peaks at 942.41 and

https://doi.org/10.1021/acsomega.3c03765
ACS Omega 2023, 8, 29663−29673

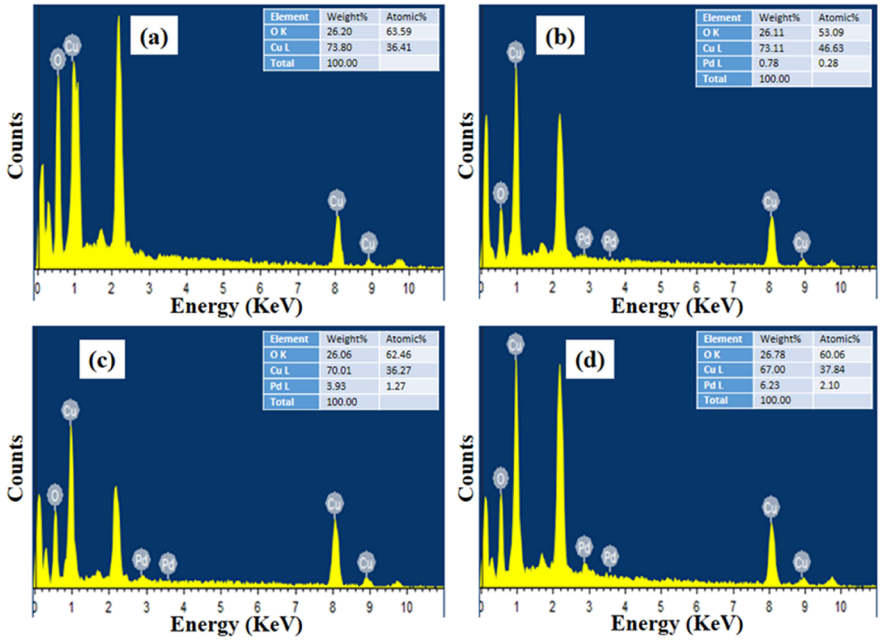

Figure 4. EDX spectra: (a) pure CuO, (b) 0.5 wt % Pd-CuO, (c) 0.8 wt % Pd-CuO, and (d) 1.12 wt % Pd-CuO.

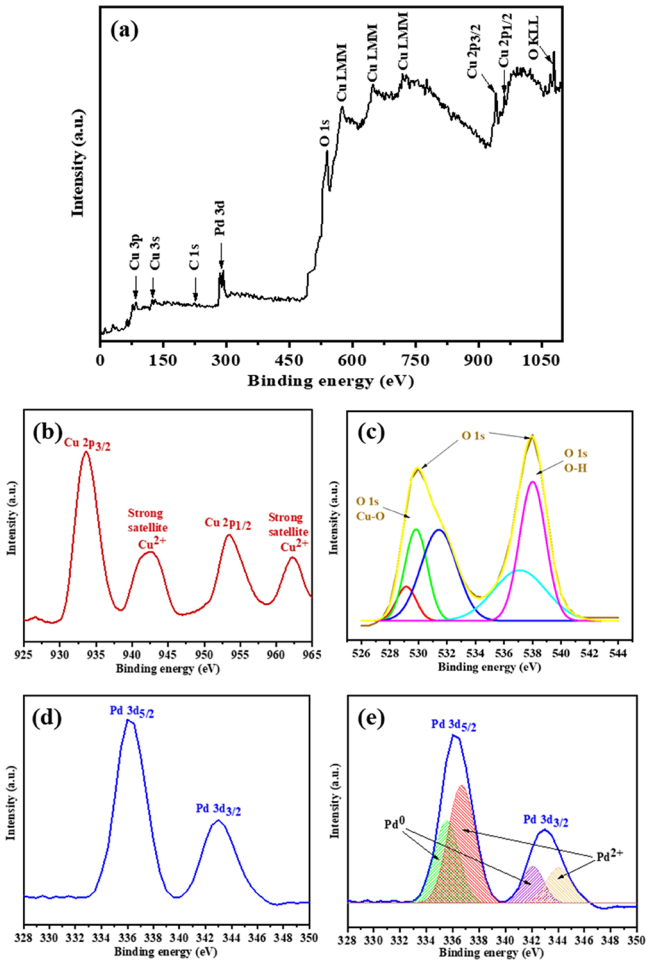

Figure 5. XPS spectrum of the Pd-CuO-3 sample: (a) survey spectrum, (b) Cu 2p, (c) O 1s, (d) Pd 3d core-level regions, and (e) deconvoluted Pd 3d region.

962.19 eV are the main features of CuO, representing the existence of Cu^{2+}.[64] Figure 5c illustrates the asymmetric XPS spectra for CuO corresponding to the O 1s core level, where five different peaks at 529.15, 529.81, 531.40, 537.04, and 537.98 eV are the reasons for the broadened peak of O 1s, in which the peak appears at 529.73 related to O 1s of Cu_2O. O 1s of CuO appeared at 534.04 eV, and the other peaks may result from the O1s of other components containing an oxygen atom in their moiety, like H_2O, OH, carbonate, or sulfate.[65] The Pd 3d XPS region is presented in Figure 5d, where the peaks at 336.07 and 342.98 eV are attributed to Pd $3d_{5/2}$ and Pd $3d_{3/2}$, respectively. A further deconvolution of the Pd 3d region was performed to obtain the corresponding subpeaks (Figure 5e). In the deconvoluted spectrum, peaks corresponding to metallic Pd^0 and Pd^{2+} are observed. Accordingly, both metallic forms of Pd coexist on the surfaces of the CuO nanoparticles.

3.2. Sensing Properties. The interaction between analyte gas molecules on the sensor surface causes the material's electrical resistance to vary. This depends on the major charge carriers in the sensing layer and the nature of the analyte gas molecules (oxidizing or reducing).[66] It is generally known that the oxidizing gases (NOx and O_3) serve as acceptors and remove the charge carriers from the sensing material. The outcome of exposing n-type sensor layers to oxidizing agents is greater electrical resistance. On the other hand, exposure to oxidizing gases reduced the electrical resistance of the p-type sensing element.[67] Equation 1 defines the sensor response for the n-type sensing layer in the case of oxidizing gases[13]

$$\text{Sensitivity}\ (\%) = \frac{R_a - R_g}{R_a} \times 100 \quad (1)$$

where R_g and R_a are, respectively, the sensor resistance values in the presence and absence of target gas molecules.

The current−voltage behavior of the Pd-CuO-3 sensor sample in dry air and 100 ppm NO_2 level at 125 °C is shown in Figure 6a. It demonstrates the ohmic behavior of the proposed sensing device. Also, it shows how the electrical resistance of

https://doi.org/10.1021/acsomega.3c03765
ACS Omega 2023, 8, 29663−29673

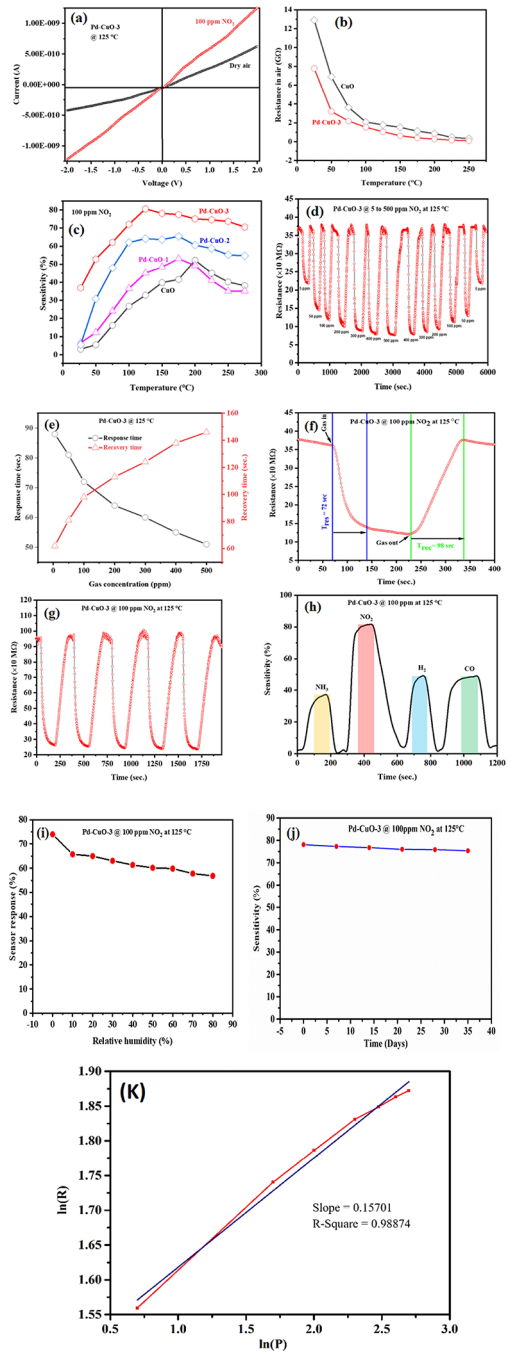

Figure 6. (a), Voltage−current graph of Pd-CuO-3 sensors in 100 ppm NO_2 gas and dry air atmosphere at 125 °C. (b) Resistance of a pure CuO and Pd-doped CuO thin-film sensor changes, as the temperature rises in dry air atmospher. (c) Response (%) of pure and Pd-doped CuO sensors at different temperatures. (d) Sensor resistance vs time curve for the Pd-CuO-3 sensor device at various NO_2 concentrations (5−500 ppm) at 125 °C. (e) Response vs time for a 5 ppm NO_2 level, with 90 and 50 s as the response and recovery times, respectively. (f) Sensor Pd-CuO-3 showing the response and recovery curves with respect to time for different concentrations (5−500 ppm) at 125 °C. (g) Cyclability curve for a Pd-doped CuO sensor up to five cycles at 100 ppm NO_2 gas in dry synthetic air. (h) Selectivity curve for the Pd-CuO-3 sensor for different gases at 100 ppm concentration at 125 °C. (i) Sensor response at different relative humidity conditions. (j) Long-term stability plot of the Pd-CuO-3 sensor. (k) Calibration curve of the Pd-CuO-3 sensor in the 5−500 ppm range of NO_2 gas for LOD.

the sensor changes in accordance with the exposure to the target gas molecules. The amount of free charge carriers that may increase on the sensor's surface after exposure to NO_2 (100 ppm) may lead to a drop in electrical conductivity, which reduces the current.[68] Figure 6b depicts how the resistance of pure CuO and Pd-CuO-3 sensors changes as the temperature rises in a dry air atmosphere. In comparison to the pure CuO-based sensor, it has been shown that the Pd-CuO-3 sensor exhibits more reduction in resistance in dry air with temperature. After the addition of Pd, the resistance of the CuO thin film decreased, and this may be attributed to the rise in conductivity and the concentration of charge carriers.[69]

The gas-sensing characteristics of all sensors at 100 ppm NO_2 level in dry air are shown in Figure 6c at various temperatures. It can be revealed that at an operating temperature of 125 °C, the Pd-CuO-3 sensor device exhibits an increasing trend in sensor response. This is because when the working temperature of the device is raised, the interaction between target gas molecules and oxygen ions escalates, potentially amplifying the sensor response. The obtained results show that the Pd-CuO thin film displays a higher sensor response than pure CuO. This might be due to Pd-CuO-3 having a large concentration of electron carriers, which increases the electrical conductivity. For the Pd-CuO-3 sensor, Figure 6c also shows that the sensor response begins to decline as the temperature raises over 125 °C. It signifies that 125 °C is the working temperature of the Pd-CuO-3 sensor. Similarly, it has been shown that 200 °C is the working temperature for pure CuO. It could be brought on by the sluggish chemical activation energy between the molecules of the adsorbed analyte gas and the sensor layer at low temperatures. Additionally, at high working temperatures, target gas molecules desorb before a chemical reaction can occur on the sensor surface.[70] The sensor resistance versus time curve for the Pd-CuO-3 sensor device at various NO_2 concentrations (5−500 ppm) at 125 °C is shown in Figure 6d. For chemiresistive gas sensors, the interaction of target gas molecules with the top surface of the detecting material causes the sensor response. These obtained results clearly demonstrate a significant improvement in the performance of the sensor with an increase in the concentration of target gas molecules. The developed sensor is able to detect 5 ppm of NO_2 in dry air at 125 °C. Pd-CuO exhibits high active surface areas, thus providing plenty of surface reaction sites to adsorb the target gas molecules and improve the detection limit.[71]

The term "response time" refers to the amount of time needed to reach up to 90% of the maximum stable signal values, whereas "recovery time" refers to the amount of time needed to recover up to 10% of the entire value of the sensor signal. Figure 6e depicts the response and recovery time behavior of the Pd-CuO-3 sensor at 125 °C for various NO_2 concentrations. These results showed that the reaction time decreased as the analyte gas concentration increased and that the recovery time improved as NO_2 gas concentration increased from 5 to 500 ppm in dry air. The response/recovery times were found to be 72 s/98 s and 90 s/50 s for 100 and 5 ppm NO_2 gas, respectively, at 125 °C, as illustrated in Figure 6f. The cyclability curve for a Pd-CuO-3 sensor up to five cycles at 100 ppm NO_2 gas in dry synthetic air is shown in Figure 6g. A nearly steady performance is seen up to the fifth cycle by the Pd-CuO-3 sensor. Consequently, it contributed to the long-term stability of the sensor device for a variety of practical applications. The sensor's cross-sensitivity measure-

https://doi.org/10.1021/acsomega.3c03765
ACS Omega 2023, 8, 29663−29673

ment at the 100 ppm concentration level of many target gases at 125 °C in dry air is shown in Figure 6h. The sensor device may be seen to have the maximum sensitivity (81.7%) to NO_2 and the minimum to other interfering gases (NH_3, CO, and H_2). It demonstrates that at 125 °C, the Pd-CuO-3 sensor device has good NO_2 gas selectivity.

Moreover, the sensor response for Pd-CuO-3 has been investigated for a range of humid conditions (relative humidity, 0−80%) at 100 ppm NO_2 at 125 °C, and the obtained results are shown in Figure 6i. The results clearly indicate the effect of humidity on the sensor performance. There is an initial decrease of 5% in the sensor's response as the level of humidity rises. Further, up to the level of 80% relative humidity, the sensor response is almost stable/uniform. The initial decrease in sensor response is mainly attributable to the adsorption of hydroxyl ions' (OH^-) on the top surface of the sensing layer under high humid conditions. This leads to a reduced number of interactions between gas molecules and surface oxygen species, and as a result, the baseline resistance decreases. Hence, the sensor's response slightly drops off.[72] Figure 6j shows the long-term stability of the Pd-CuO-3 sensor for the duration of 35 days, and the response of this sensor presents remarkable long-term stability with no discernible drift. As a function of NO_2 gas concentration, the sensor's response constantly rises in accordance with the power law ($R = aP^n$ or $\ln R = C_0 + n\ln P$), where a and C_0 are constants. The partial pressure of the gas NO_2 is P, and R stands for sensor resistance, while n, commonly known as sensitivity, stands for power law exponents. Additionally, as shown in Figure 6k, the sensitivity (i.e., slope), which represents the change in response with respect to the analyte gas concentration, was calculated as the slope of the linear fit on the curves. For the Pd-CuO-3 sensor, the power law exponent n and the coefficient of determination (R^2) values were calculated to be 0.15701 and 0.98874, respectively. In addition, the limit of detection (LOD) was projected from the experimental data by employing the equation LOD = 3.3 × RMS_{noise}/slope, where RMS_{noise} is the root-mean-square (RMS) deviation of the baseline, before the exposure to the target gas.[15] The calculated LOD value is 0.8235 for the Pd-CuO-3 sensor toward NO_2. This appealing LOD is suitable for real-time gas detection. Additionally, a quantitative examination of cross-selectivity, which is determined by the ratio of the response of the target gas to the interfering gases, was done.[13] S_{NO_2}/S_{NH_3}, S_{NO_2}/S_{H_2}, and S_{NO_2}/S_{CO} ratios were seen to be, 0.4621, 0.59906, and 0.6006, respectively. This shows that NH_3, H_2, and CO do not interact as much with NO_2 at 125 °C as NO_2.

4. SENSING MECHANISM

The sensing mechanism of the Pd-doped CuO-based gas sensor can be explained by the change in resistance caused by the reaction and adsorption/desorption of gas molecules on the surface of semiconductor.[32] When a CuO sensor is exposed to air, oxygen molecules become adsorbed on its surface and are prepared to be ionized by electrons to form adsorbed oxygen species (O^{2-}, O^-, and O^{2-}), as demonstrated in eqs 2−5. In this procedure, the capture of electrons causes an accumulation of holes close to the CuO surface. When the sensor is exposed to NO_2 gas, The NO_2 molecules tend to accept electrons from the CuO, leading to the formation of oxygen vacancies (O^-) and NO_2^- within the CuO lattice, as demonstrated in eqs 6 and 7. The formation of oxygen vacancies (O^-) and NO_2^- in the CuO lattice increases the concentration of holes in the material, resulting in enhancing the concentration of holes reduces the resistance of the Pd-doped CuO sensor[73−75]

$$O_2\ (gas) \rightarrow O_2\ (ads) \tag{2}$$

$$O_2\ (ads) + e^- \rightarrow O_2^-\cdot(ads) \tag{3}$$

$$O_2^-\cdot(ads) + e^- \rightarrow 2O^-\cdot(ads) \tag{4}$$

$$O^-\cdot(ads) + e^- \rightarrow O^{2-}\cdot(ads) \tag{5}$$

$$NO_2\ (gas) + e^- \rightarrow NO_2(ads) \tag{6}$$

$$NO_2\ (ads) + O_2^- + 2e^- \rightarrow NO_2^-\ (ads) + 2O^-\ (ads) \tag{7}$$

The doping process could improve the sensing performance, as shown in Figure 7. The electronic and chemical sensitization

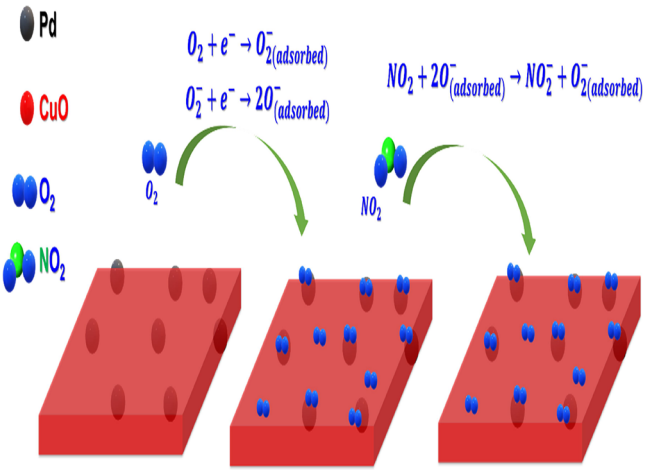

Figure 7. Schematic diagram illustrating the sensing mechanism of the Pd-CuO sensor.

are two types of mechanisms that are mainly responsible for the enhanced response to the Pd-CuO sensor.[76,77] According to the chemical sensitization, PdO is also a p-type material with good conductivity and a higher intrinsic carrier concentration than other materials. This might be one of the primary causes of Pd doping, which lowers the operating temperature of Pd-CuO sensors. Additionally, the catalytic properties of Pd can encourage to capture more oxygen molecules by the sensing material, resulting in enhancing the sensor's response.[78] The electronic sensitization is also responsible to increase the response of Pd-CuO sensors.[79,89] According to electronic sensing, when NO_2 gas is exposed to the sensor, the Pd molecules on the surface of CuO participate in the reaction and release electrons. These electrons recombine with the holes and reduce the hole concentration; consequently, the Pd-CuO sensor's resistance decreases when exposed to NO_2 gas. In a word, Pd doping is generally responsible for the improved response of the CuO sensor. The comparison between the NO_2 sensing performance of the various CuO-based sensors in this study and those reported in the literature is summarized in Table 1. The Pd-doped CuO sensor performance is comparable to or better than that of other developed sensors.

https://doi.org/10.1021/acsomega.3c03765
ACS Omega 2023, 8, 29663−29673

Table 1. NO_2 Sensing Performance of the Various CuO-Based Sensors

materials	morphology	NO_2 concentration (ppm)	operating temperature (°C)	response (S)	response/recovery time (s)	ref.
CuO	nanocubes	100	150	76%	6/1200	80
CuO	nanoplatelets	20	50	14.5	−/−	33
CuO	nanoplatelets	40	RT	2498%	−/−	81
CuO−ZnO	nanocomposites	100	200	73%	6/−	35
CuO/ZnO	heterostructure	5	RT	337%	18/32	37
Cu_2O/CuO	mulberry-like nanocomposites	0.1	RT	62.3%	58/250	38
CuO	nanosheets/(MEMS)	0.05	23.2	25.8%	−/−	19
CuO	urchin-like NPs	50	250	1.9	−/−	82
CuO	thin film	5	200	56%	20.5/235.2	17
ZnO/CuO	heterostructure	100	150	71%	12/219	83
CuO-In_2O_3	hollow sphere	300 ppb	100	430	430/170	84
In_2O_3-CuO	thin film	193	200	89.77%	24/24	85
CuO−TiO_2	thin film	20	150	∼1.2	482/574	86
Au-CuO	nanowires	1	300	60	−/−	87
Cr-CuO	nanorods	100	250	134.2	55/1642	88
Pd (1.12 wt %) doped-CuO	**nanobars**	**100**	**125**	**81.7%**	**72/98**	**Present work**
		5	**125**	**38.9%**	**90/50**	

5. CONCLUSIONS

The green synthesis method was used to prepare a gas sensor based on Pd-CuO nanostructure for NO_2 detection. All characterization results confirm the successful doping of Pd^{2+} ions into the CuO matrix. At the doping concentration of Pd (1.12 wt %), the sensor yields the maximum and fast response for 100 ppm NO_2 at low temperature. Moreover, when the NO_2 concentration is as low as 5 ppm, the response of the sensor is still good, and the response/recovery time is acceptable. Besides, the response of the sensor is almost stable for the increased level of relative humidity upto 80%. The obtained results indicate that Pd doping plays a significant role in improving the sensing performance of the prepared sensor for NO_2 gas. Thus, the Pd (1.25 wt %)-doped CuO-based sensor provides good sensitivity, good selectivity, excellent reversibility, and superior long-term stability for NO_2 gas at a low operating temperature and henceforth can be categorized as a potential NO_2 gas sensor. The present biosynthesized Pd-CuO-based sensor shows remarkable gas-sensing performance toward NO_2 and implicative to make an ecofriendly outcome in the future. The green-synthesized gas sensors pave the way for an alternative route to protect the environment by detecting the toxic gases without inducing less noxious waste. Furthermore, usage of less hazardous solvents minimizes the harmful effects on the human health and consumes least energy.

AUTHOR INFORMATION

Corresponding Authors

Yogendra K. Gautam − *Smart Materials and Sensor Laboratory, Department of Physics, Chaudhary Charan Singh University, Meerut, Uttar Pradesh 250004, India;* orcid.org/0000-0003-4662-4583; Email: ykg.iitr@gmail.com

Ashwani Kumar − *Institute Instrumentation Centre, Indian Institute of Technology Roorkee, Roorkee, Uttrakhand 247667, India; Department of Physics, Graphic Era (Deemed to be University), Dehradun, Uttarakhand 248002, India;* Email: 01ashraj@gmail.com

Authors

Anit K. Ambedkar − *Smart Materials and Sensor Laboratory, Department of Physics, Chaudhary Charan Singh University, Meerut, Uttar Pradesh 250004, India*

Durvesh Gautam − *Smart Materials and Sensor Laboratory, Department of Physics, Chaudhary Charan Singh University, Meerut, Uttar Pradesh 250004, India*

Sagar Vikal − *Smart Materials and Sensor Laboratory, Department of Physics, Chaudhary Charan Singh University, Meerut, Uttar Pradesh 250004, India*

Manohar Singh − *Smart Materials and Sensor Laboratory, Department of Physics, Chaudhary Charan Singh University, Meerut, Uttar Pradesh 250004, India*

Amit Sanger − *Department of Physics, Netaji Subhas University of Technology, New Delhi 110078, India;* orcid.org/0000-0002-1287-4253

Kavita Sharma − *Smart Materials and Sensor Laboratory, Department of Physics, Chaudhary Charan Singh University, Meerut, Uttar Pradesh 250004, India*

Beer Pal Singh − *Smart Materials and Sensor Laboratory, Department of Physics, Chaudhary Charan Singh University, Meerut, Uttar Pradesh 250004, India;* orcid.org/0000-0002-1646-8404

Complete contact information is available at: https://pubs.acs.org/10.1021/acsomega.3c03765

Notes

The authors declare no competing financial interest.

ACKNOWLEDGMENTS

The authors thank Prof. Ramesh Chandra, IIC, IIT Roorkee, India, for providing XRD, XPS, and FESEM facilities to carry out this research work. The authors also thank DST, Govt. of India, for providing a FIST grant for sputtering and SEM. This work was supported by the UGC, Govt. of India [No.F.30−303/2016 (BSR) and F.D.Dy. No. 11299], and CCS University, Meerut [DEV/URGS/2022-23/39].

https://doi.org/10.1021/acsomega.3c03765
ACS Omega 2023, 8, 29663−29673

REFERENCES

(1) Tamvakos, A.; Korir, K.; Tamvakos, D.; Calestani, D.; Cicero, G.; Pullini, D. NO2 Gas Sensing Mechanism of ZnO Thin-Film Transducers: Physical Experiment and Theoretical Correlation Study. *ACS Sens.* **2016**, *1*, 406−412.

(2) Gautam, Y. K.; Sharma, K.; Tyagi, S.; Ambedkar, A. K.; Chaudhary, M.; Pal Singh, B. Nanostructured metal oxide semiconductor-based sensors for greenhouse gas detection: Progress and challenges. *R. Soc. Open Sci.* **2021**, *8*, No. 201324.

(3) Ding, J.; et al. Aerosol assisted chemical vapour deposition of nanostructured ZnO thin films for NO2 and ethanol monitoring. *Ceram. Int.* **2020**, *46*, 15152−15158.

(4) Zhang, Y. H.; Li, Y. L.; Gong, F. L.; Xie, K. F.; Liu, M.; Zhang, H. L.; Fang, S. M. Al doped narcissus-like ZnO for enhanced NO2 sensing performance: An experimental and DFT investigation. *Sens. Actuators B: Chem.* **2020**, *305*, No. 127489.

(5) Jin, C.; et al. Characterization and gas sensing properties of bead-like ZnO using multi-walled carbon nanotube templates. *Ceram. Int.* **2015**, *41*, 7729−7734.

(6) Baratto, C.; Sberveglieri, G.; Onischuk, A.; Caruso, B.; Di Stasio, S. Low temperature selective NO2 sensors by nanostructured fibres of ZnO. *Sens. Actuators B: Chem.* **2004**, *100*, 261−265.

(7) Richters, A.; Kuraitis, K. Inhalation of NO2 and blood borne cancer cell spread to the lungs. *Arch. Environ. Health* **1981**, *36*, 36−39.

(8) Bai, S.; Sun, X.; Han, N.; Shu, X.; Pan, J.; Guo, H.; Liu, S.; Feng, Y.; Luo, R.; Li, D.; Chen, A. rGO modified nanoplate-assembled ZnO/CdO junction for detection of NO2. *J. Hazard. Mater.* **2020**, *394*, No. 121832.

(9) Tyagi, S.; et al. Enhancement in the sensitivity and selectivity of Cu functionalized MoS2 nanoworm thin films for nitrogen dioxide gas sensor. *Mater. Res. Bull.* **2022**, *150*, No. 111784.

(10) Wang, D.; Zhang, D.; Mi, Q. A high-performance room temperature benzene gas sensor based on CoTiO 3 covered TiO 2 nanospheres decorated with Pd nanoparticles. *Sens. Actuators B: Chem.* **2022**, *350*, No. 130830.

(11) Wang, D.; Zhang, D.; Pan, Q.; Wang, T.; Chen, F. Gas sensing performance of carbon monoxide sensor based on rod-shaped tin diselenide / MOFs derived zinc oxide polyhedron at room temperature. *Sens. Actuators B: Chem.* **2022**, *371*, No. 132481.

(12) Wang, D.; Zhang, D.; Tang, M.; Zhang, H.; Sun, T.; Yang, C.; Mao, R.; Li, K.; Wang, J. Nanogenerator driven self - powered MXene-based sensor system for marine environmental monitoring. *Nano Energy* **2022**, *100*, No. 107509.

(13) Maake, P. J.; Mokoena, T. P.; Bolokang, A. S.; Hintsho-mbita, N.; Tshilongo, J.; Cummings, F. R.; Swart, H. C.; Iwuoha, E. I.; Motaung, D. E. Fabrication of AgCu/TiO_2 nanoparticle-based sensors for selective detection of xylene vapor. *Mater. Adv.* **2022**, *3*, 7302−7318.

(14) Wang, D.; Zhang, D.; Yang, Y.; Mi, Q.; Zhang, J.; Yu, L. Multifunctional Latex/Polytetrafluoroethylene-Based Triboelectric Nanogenerator for Self-Powered Organ-like MXene/Metal−Organic Framework-Derived CuO Nanohybrid Ammonia Sensor. *ACS Nano* **2021**, *15*, 2911−2919.

(15) Tshabalala, Z. P.; Mokoena, T. P.; Jozela, M.; Tshilongo, J.; Hillie, T. K.; Swart, H. C.; Motaung, D. E. TiO_2 Nanowires for Humidity-Stable Gas Sensors for Toluene and Xylene. *ACS Appl. Nano Mater.* **2021**, *4*, 702−716.

(16) Sik Choi, M.; et al. Selective, sensitive, and stable NO2 gas sensor based on porous ZnO nanosheets. *Appl. Surf. Sci.* **2021**, *568*, No. 150910.

(17) Khot, S.; Phalake, S.; Mahadik, S.; Baragale, M.; Jagadale, S.; Burungale, V.; Navale, Y.; Patil, V.; Patil, V.; Patil, P.; Patil, S. Synthesis of cuo thin film sensors by spray pyrolysis method for no2 gas detection. *Mater. Today Proc.* **2021**, *43*, 2694−2697.

(18) Mohanta, D.; Ahmaruzzaman, M. Novel Ag-SnO2-βC3N4 ternary nanocomposite based gas sensor for enhanced low-concentration NO2 sensing at room temperature. *Sens. Actuators B: Chem.* **2021**, *326*, No. 128910.

(19) Hou, J. L.; Hsueh, T. J. Temperature-Dependent n-Type and p-Type Sensing Behaviors of CuO Nanosheets/MEMS to NO2Gas. *ACS Appl. Electron. Mater.* **2021**, *3*, 4817−4823.

(20) Hung, N. M.; et al. Carbon nanotube-metal oxide nanocomposite gas sensing mechanism assessed via NO2 adsorption on n-WO3/p-MWCNT nanocomposites. *Ceram. Int.* **2020**, *46*, 29233−29243.

(21) Jaiswal, J.; Singh, P.; Chandra, R. Low-temperature highly selective and sensitive NO 2 gas sensors using CdTe-functionalized ZnO filled porous Si hybrid hierarchical nanostructured thin films. *Sens. Actuators B: Chem.* **2021**, *327*, No. 128862.

(22) Munusami, V.; Arutselvan, K.; Vadivel, S. Development of high sensitivity LPG and NO2 gas sensor based ZnGa2O4/graphene nanoplates hybrid structure - A novel approach. *Diam. Relat. Mater.* **2021**, *111*, No. 108167.

(23) Gawali, S. R.; et al. Ce doped NiO nanoparticles as selective NO2 gas sensor. *J. Phys. Chem. Solids* **2018**, *114*, 28−35.

(24) Khudadad, A. I.; Yousif, A. A.; Abed, H. R. Effect of heat treatment on WO3 nanostructures based NO2 gas sensor low-cost device. *Mater. Chem. Phys.* **2021**, *269*, No. 124731.

(25) Mirzaei, S.; Ghabooli, A.; Mirzaei, M. Botrytis Cinerea, One of the Most Destructive Plant Pathogens, as a Potent to Produce Silver Nanoparticles. *Int. J. Nanosci. Nanotechnol.* **2020**, *16*, 243−248.

(26) Oosthuizen, D. N.; Motaung, D. E.; Swart, H. C. In depth study on the notable room-temperature NO2 gas sensor based on CuO nanoplatelets prepared by sonochemical method: Comparison of various bases. *Sens. Actuators B: Chem.* **2018**, *266*, 761−772.

(27) Yathisha, R. O.; Arthoba Nayaka, Y. Structural, optical and electrical properties of zinc incorporated copper oxide nanoparticles: doping effect of Zn. *J. Mater. Sci.* **2018**, *53*, 678−691.

(28) Siddiqui, H.; Qureshi, M. S.; Haque, F. Z. Valuation of copper oxide (CuO) nanoflakes for its suitability as an absorbing material in solar cells fabrication. *Optik* **2016**, *127*, 3713−3717.

(29) Li, X.; Guo, W.; Liu, Y.; He, W.; Xiao, Z. Spinel LiNi0.5Mn1.5O4 as superior electrode materials for lithium-ion batteries: Ionic liquid assisted synthesis and the effect of CuO coating. *Electrochim. Acta* **2014**, *116*, 278−283.

(30) Etefagh, R.; Azhir, E.; Shahtahmasebi, N. Synthesis of CuO nanoparticles and fabrication of nanostructural layer biosensors for detecting Aspergillus niger fungi. *Sci. Iran.* **2013**, *20*, 1055−1058.

(31) Sharma, A.; Varshney, M.; Ha, T. K.; Chae, K. H.; Shin, H. J. X-ray absorption spectroscopy study and photocatalyst application of CuO and Cu0.9Ti0.1O nanoparticles. *Curr. Appl. Phys.* **2015**, *15*, 1148−1155.

(32) Yang, C.; Xiao, F.; Wang, J.; Su, X. 3D flower- and 2D sheet-like CuO nanostructures: Microwave-assisted synthesis and application in gas sensors. *Sens. Actuators B: Chem.* **2015**, *207*, 177−185.

(33) Oosthuizen, D. N.; Korditis, I.; Swart, H. C.; Motaung, D. E. Facile control of room temperature nitrogen dioxide gas selectivity induced by copper oxide nanoplatelets. *J. Colloid Interface Sci.* **2020**, *560*, 755−768.

(34) Oosthuizen, D. N.; Motaung, D. E.; Strydom, A. M.; Swart, H. C. Underpinning the Interaction between NO_2 and CuO Nanoplatelets at Room Temperature by Tailoring Synthesis Reaction Base and Time. *ACS Omega* **2019**, *4*, 18035−18048.

(35) Mali, S. M.; Narwade, S. S.; Navale, Y. H.; Tayade, S. B.; Digraskar, R. V.; Patil, V. B.; Kumbhar, A. S.; Sathe, B. R. Heterostructural cuo-zno nanocomposites: A highly selective chemical and electrochemical NO_2 sensor. *ACS Omega* **2019**, *4*, 20129−20141.

(36) Gomaa, M. M.; Sayed, M. H.; Patil, V. L.; Boshta, M.; Patil, P. S. Gas sensing performance of sprayed NiO thin films toward NO2 gas. *J. Alloys Compd.* **2021**, *885*, No. 160908.

(37) Govind, A.; Bharathi, P.; Mohan, M. K.; Archana, J.; Harish, S.; Navaneethan, M. Highly sensitive near room temperature operable NO2 gas-sensor for enhanced selectivity via nanoporous CuO@ZnO heterostructures. *J. Environ. Chem. Eng.* **2023**, *11*, No. 110056.

https://doi.org/10.1021/acsomega.3c03765
ACS Omega 2023, 8, 29663−29673

(38) Ni, M.; et al. Enhanced room-temperature NO2 sensing performance of mulberry-like Cu2O/CuO composites. *Sens. Actuators A: Phys.* **2023**, *350*, No. 114136.
(39) Dudhane, A. A.; Waghmode, S. R.; Dama, L. B.; Mhaindarkar, V. P.; Sonawane, A.; Katariya, S. Synthesis and characterization of gold nanoparticles using plant extract of Terminalia arjuna with antibacterial activity. *Int. J. Nanosci. Nanotechnol.* **2019**, *15*, 75−82.
(40) Saranya, S.; Vijayaranai, K.; Pavithra, S.; Raihana, N.; Kumanan, K. In vitro cytotoxicity of zinc oxide, iron oxide and copper nanopowders prepared by green synthesis. *Toxicol. Rep.* **2017**, *4*, 427−430.
(41) Pal, S.; Mondal, S.; Maity, J.; Mukherjee, R. Synthesis and characterization of zno nanoparticles using Moringa Oleifera leaf extract: Investigation of photocatalytic and antibacterial activity. *Int. J. Nanosci. Nanotechnol.* **2018**, *14*, 111−119.
(42) Dadkhah, M.; Tulliani, J.-M. Green Synthesis of Metal Oxides Semiconductors for Gas Sensing Applications. *Sensors (Basel)* **2022**, *22*, 4669.
(43) Ananda Murthy, H. C.; Abebe, B.; C H, P.; Shantaveerayya, K. A Review on Green Synthesis and Applications of Cu and CuO Nanoparticles. *Mater. Sci. Res. India* **2018**, *15*, 279−295.
(44) Phukan, S.; Kakati, D.; Rashid, M. H. Use of Invasive Weed to Synthesize Shape-Tunable Gold Nanoparticles and Evaluation of their Catalytic Activities in Dye Reduction. *Curr. Nanosci.* **2018**, *14*, 511−519.
(45) Keabadile, O. P.; Aremu, A. O.; Elugoke, S. E.; Fayemi, O. E. Green and traditional synthesis of copper oxide nanoparticles—comparative study. *Nanomaterials* **2020**, *10*, 2502.
(46) Naika, H. R.; Lingaraju, K.; Manjunath, K.; Kumar, D.; Nagaraju, G.; Suresh, D.; Nagabhushana, H. Green synthesis of CuO nanoparticles using Gloriosa superba L. extract and their antibacterial activity. *J. Taibah Univ. Sci.* **2015**, *9*, 7−12.
(47) Chowdhury, R.; Mollick, M. M. R.; Biswas, Y.; Chattopadhyay, D.; Rashid, M. H. Biogenic synthesis of shape-tunable Au-Pd alloy nanoparticles with enhanced catalytic activities. *J. Alloys Compd.* **2018**, *763*, 399−408.
(48) Muthuvel, A.; Jothibas, M.; Manoharan, C. Synthesis of copper oxide nanoparticles by chemical and biogenic methods: photocatalytic degradation and in vitro antioxidant activity. *Nanotechnol. Environ. Eng.* **2020**, *5*, 14.
(49) Phukan, S.; Mahanta, A.; Kakati, D.; Rashid, M. H. Green chemical synthesis of Pd nanoparticles for use as efficient catalyst in Suzuki-Miyaura cross-coupling reaction. *Appl. Organomet. Chem.* **2019**, *33*, No. e4758.
(50) Arunkumar, B.; Johnson Jeyakumar, S.; Jothibas, M. A sol-gel approach to the synthesis of CuO nanoparticles using Lantana camara leaf extract and their photo catalytic activity. *Optik* **2019**, *183*, 698−705.
(51) Małolepsza, J.; Joachimiak, Ł.; Błazewska, K. M. Aza-Michael Addition of Imidazole Analogues. *Synthesis* **2016**, *48*, 2681−2704.
(52) *Sensors for environment, health and security: Advanced Materials and Technologies*, Baraton, M-I, Ed. Vichy (France) 16−27 September 2007, Springer: Netherland.
(53) Zhang, D. E.; Ni, X. M.; Zheng, H. G.; Li, Y.; Zhang, X. J.; Yang, Z. P. Synthesis of needle-like nickel nanoparticles in water-in-oil microemulsion. *Mater. Lett.* **2005**, *59*, 2011−2014.
(54) Chowdhury, R.; Khan, A.; Rashid, M. H. Green synthesis of CuO nanoparticles using: Lantana camara flower extract and their potential catalytic activity towards the aza-Michael reaction. *RSC Adv.* **2020**, *10*, 14374−14385.
(55) Goutham, S.; Kaur, S.; Sadasivuni, K. K.; Bal, J. K.; Jayarambabu, N.; Kumar, D. S.; Rao, K. V. Nanostructured ZnO gas sensors obtained by green method and combustion technique. *Mater. Sci. Semicond. Process.* **2017**, *57*, 110−115.
(56) Gattu, K. P.; Ghule, K.; Kashale, A. A.; Patil, V. B.; Phase, D. M.; Mane, R. S.; Han, S. H.; Sharma, R.; Ghule, A. V. Bio-Green Synthesis of Ni doped Tin Oxide Nanoparticles and its Influence on Gas Sensing Properties. *RSC Adv.* **2015**, *5*, 72849−72856.
(57) Gattu, K. P.; et al. NO2 sensing studies of bio-green synthesized Au-doped SnO2. *J. Mater. Sci.: Mater. Electron.* **2017**, *28*, 13209−13216.
(58) Nagar, A.; et al. Ultrafast, trace-level detection of NH3 gas at room temperature using hexagonal-shaped ZnO nanoparticles grown by novel green synthesis technique. *Phys. B: Condens. Matter* **2022**, *626*, No. 413595.
(59) Poonguzhali, R. V.; et al. Natural lemon extract assisted green synthesis of spinel Co3O4 nanoparticles for LPG gas sensor application. *Sens. Actuators B: Chem.* **2023**, *377*, No. 133036.
(60) Krishnakumar, T.; Jayaprakash, R.; Pinna, N.; Donato, N.; Bonavita, A.; Micali, G.; Neri, G. CO gas sensing of ZnO nanostructures synthesized by an assisted microwave wet chemical route. *Sens. Actuators B: Chem.* **2009**, *143*, 198−204.
(61) Ambedkar, A. K.; et al. Structural, optical and thermoelectric properties of Al-doped ZnO thin films prepared by spray pyrolysis. *Surf. Interfaces* **2020**, *19*, No. 100504.
(62) Vomáčka, P.; Štengl, V.; Henych, J.; Kormunda, M. Shape-controlled synthesis of Sn-doped CuO nanoparticles for catalytic degradation of Rhodamine B. *J. Colloid Interface Sci.* **2016**, *481*, 28−38.
(63) Singh, M.; et al. Room temperature photoluminescence and spectroscopic ellipsometry of reactive co-sputtered Cu-doped ZnO thin films. *Optik* **2022**, *257*, No. 168860.
(64) Wang, S. R. Y.; Qu, F.; Liu, J.; Wang, Y.; Zhou, J.; Ruan, S. Enhanced H2S sensing characteristics of CuO-NiO core-shell microspheres sensors. *Sens. Actuators B. Chem.* **2015**, *209*, 515−523.
(65) Wang, C.; et al. Ultrasensitive and low detection limit of acetone gas sensor based on W-doped NiO hierarchical nanostructure. *Sens. Actuators B. Chem.* **2015**, *220*, 59−67.
(66) Kim, K. S.; Chung, G. S. Characterization of porous cubic silicon carbide deposited with Pd and Pt nanoparticles as a hydrogen sensor. *Sens. Actuators B: Chem.* **2011**, *157*, 482−487.
(67) Wang, C.; Yin, L.; Zhang, L.; Xiang, D.; Gao, R. Metal Oxide Gas Sensors: Sensitivity and Influencing Factors. *Sensors (Basel).* **2010**, *10*, 2088−2106.
(68) Wang, J. X.; Sun, X. W.; Yang, Y.; Wu, C. M. L. N-P transition sensing behaviors of ZnO nanotubes exposed to NO2 gas. *Nanotechnology* **2009**, *20*, No. 465501.
(69) Eğri, O. Production of lavender oil loaded antibacterial polymeric membranes. *Cumhur. Sci. J.* **2020**, *41*, 160−168.
(70) Liu, L.; Li, S.; Zhuang, J.; Wang, L.; Zhang, J.; Li, H.; Liu, Z.; Han, Y.; Jiang, X.; Zhang, P. Improved selective acetone sensing properties of Co-doped ZnO nanofibers by electrospinning. *Sens. Actuators B Chem.* **2011**, *155*, 782−788.
(71) Agrawal, A. V.; Kumar, N.; Kumar, M. Strategy and Future Prospects to Develop Room-Temperature-Recoverable NO2 Gas Sensor Based on Two-Dimensional Molybdenum Disulfide. *Nanomicro Lett.* **2021**, *13*, 38. Springer Singapore.
(72) Chen, J.; Zhang, J.; Wang, M.; Li, Y. High-temperature hydrogen sensor based on platinum nanoparticle-decorated SiC nanowire device. *Sens. Actuators B Chem.* **2014**, *201*, 402−406.
(73) Jyoti; Varma, G. D. Enhanced room temperature sensitivity of Ag-CuO nanobrick/reduced graphene oxide composite for NO2. *J. Alloys Compd.* **2019**, *806*, 1469−1480.
(74) Zhang, D.; Jiang, C.; Liu, J.; Cao, Y. Carbon monoxide gas sensing at room temperature using copper oxide-decorated graphene hybrid nanocomposite prepared by layer-by-layer self-assembly. *Sens. Actuators B Chem.* **2017**, *247*, 875−882.
(75) Jiang, C.; Zhang, D.; Yin, N.; Yao, Y.; Shaymurat, T.; Zhou, X. Acetylene gas-sensing properties of layer-by-layer self-assembled Ag-decorated tin dioxide/graphene nanocomposite film. *Nanomaterials* **2017**, *7*, 278.
(76) Zhang, Y.; Zheng, Z.; Yang, F. Highly sensitive and selective alcohol sensors based on Ag-doped In 2O3 coating. *Ind. Eng. Chem. Res.* **2010**, *49*, 3539−3543.
(77) Liu, Y. L.; et al. Hydrogen sulfide sensing properties of NiFe2O4 nanopowder doped with noble metals. *Sens. Actuators B Chem.* **2004**, *102*, 148−154.

https://doi.org/10.1021/acsomega.3c03765
ACS Omega 2023, 8, 29663−29673

(78) Kolmakov, A.; Klenov, D. O.; Lilach, Y.; Stemmer, S.; Moskovits, M. Enhanced gas sensing by individual SnO 2 nanowires and nanobelts functionalized with Pd catalyst particles. *Nano Lett.* **2005**, *5*, 667−673.
(79) Wei, S.; Yu, Y.; Zhou, M. CO gas sensing of Pd-doped ZnO nanofibers synthesized by electrospinning method. *Mater. Lett.* **2010**, *64*, 2284−2286.
(80) Navale, Y. H.; et al. Rapid synthesis strategy of CuO nanocubes for sensitive and selective detection of NO2. *J. Alloys Compd.* **2017**, *708*, 456−463.
(81) Oosthuizen, D. N.; Motaung, D. E.; Strydom, A. M.; Swart, H. C. Underpinning the Interaction between NO2 and CuO Nanoplatelets at Room Temperature by Tailoring Synthesis Reaction Base and Time. *ACS Omega* **2019**, *4*, 18035−18048.
(82) Volanti, D. P.; et al. The role of hierarchical morphologies in the superior gas sensing performance of CuO-based chemiresistors. *Adv. Funct. Mater.* **2013**, *23*, 1759−1766.
(83) Navale, Y. H.; Navale, S. T.; Stadler, F. J.; Ramgir, N. S.; Patil, V. B. Enhanced NO2 sensing aptness of ZnO nanowire/CuO nanoparticle heterostructure-based gas sensors. *Ceram. Int.* **2019**, *45*, 1513−1522.
(84) Zhang, C.; Huan, Y.; Sun, D.; Lu, Y. Synthesis and NO2 sensing performances of CuO nanoparticles loaded In2O3 hollow spheres. *J. Alloys Compd.* **2020**, *842*, No. 155857.
(85) Hmeed, A. A. A.; Al-Jumaili, H. S. NO_2 gas sensor properties of In_2O_3-CuO Nanocomposite thin films prepared by chemical spray pyrolysis. *IOP Conf. Ser. Mater. Sci. Eng.* **2021**, *1095*, No. 012008.
(86) Maziarz, W. TiO2/SnO2 and TiO2/CuO thin film nanoheterostructures as gas sensors. *Appl. Surf. Sci.* **2019**, *480*, 361−370.
(87) Lee, J. S.; Katoch, A.; Kim, J. H.; Kim, S. S. Effect of Au nanoparticle size on the gas-sensing performance of p-CuO nanowires. *Sens. Actuators B Chem.* **2016**, *222*, 307−314.
(88) Kim, K. M.; Jeong, H. M.; Kim, H. R.; Choi, K.-I.; Kim, H. J.; Lee, J. H. Selective Detection of NO2 Using Cr-Doped CuO Nanorods. *Sensors (Basel)* **2012**, *12*, 8013−8025.
(89) Hu, X.; Zhu, Z.; Chen, C.; Wen, T.; Zhao, X.; Xie, L. Highly sensitive H2S gas sensors based on Pd-doped CuO nanoflowers with low operating temperature. *Sens. Actuators B: Chem.* **2017**, *253*, 809−817.

NOTE ADDED AFTER ASAP PUBLICATION

This paper originally published ASAP on August 2, 2023. A correction was made in the first paragraph of the Conclusions and a new version reposted on August 2, 2023.

https://doi.org/10.1021/acsomega.3c03765
ACS Omega 2023, 8, 29663−29673